Discrete Element Simulation for Pneumatic Conveying of Granular Material

Eldin Wee Chuan Lim, and Chi-Hwa Wang
Dept. of Chemical and Biomolecular Engineering, National University of Singapore, 4 Engineering Drive 4, Singapore 117576

Ai-Bing Yu
Centre for Simulation and Modelling of Particulate Systems, School of Materials Science and Engineering, The University of New South Wales, Sydney, NSW 2052, Australia

DOI 10.1002/aic.10645
Published online September 19, 2005 in Wiley InterScience (www.interscience.wiley.com).

The pneumatic transport of granular material is a common operation frequently employed to transport solid particles from one location to another. It is well established in the literature that different flow regimes can arise in such transportation processes depending on the system geometry and operating conditions used. In this study, the pneumatic transports of solid particles in both vertical and horizontal conveying lines were studied numerically using the discrete element method coupled with computational fluid dynamics. The simulation outputs corresponded well with reported experimental observations in terms of the different flow regimes obtained at different operating conditions. In the vertical pneumatic conveying simulations, two different flow patterns corresponding to the experimentally observed dispersed flow and plug flow regimes were obtained at different gas velocities and solid concentrations. Similarly, the homogeneous flow, stratified flow, moving dunes, and slug flow regimes previously reported to occur in horizontal pneumatic conveying were also reproduced computationally in this study. Solid concentration profiles obtained by spatial averaging along the length of the pipe showed a symmetrical but non-uniform distribution for dispersed flow and an almost flat distribution for plug flow in vertical pneumatic conveying. The profile for stratified flow in horizontal pneumatic conveying showed higher solid concentration near the bottom wall due to the effects of gravitational settling, while that for slug flow was flat. Hysteresis in solid flow rates was observed in vertical pneumatic conveying near the point where transition between the dispersed and plug flow regimes was expected to occur. Solid flow rates were also found to be more sensitive towards the coefficient of friction than the coefficient of restitution of particles and the pipe walls in a sensitivity analysis study of these parameters. © 2005 American Institute of Chemical Engineers *AIChE J,* 52: 496–509, 2006
Keywords: numerical simulation, discrete element method, computational fluid dynamics, pneumatic conveying, flow regimes

Introduction

Gas-solid systems are commonly encountered in the chemical and petrochemical, food and mineral processing, and pharmaceutical industries. Their applications include fluid catalytic cracking, drying operations, mixing and granulation, and the transport of granular material and fine powders through pipelines. In particular, the pneumatic transport of granular material is a common operation frequently employed to transport solid particles from one location to another. Some of the advantages associated with this method of solid transportation include relatively high levels of safety, low operational costs, flexibility

Correspondence concerning this article should be addressed to Chi-Hwa Wang at chewch@nus.edu.sg.

of layout, ease of automation and installation, and low maintenance requirements. On the other hand, one of the main disadvantages of pneumatic transport is the occurrence of attrition of the granular material, especially at high conveying velocities. This may result in severe degradation of product quality in certain industrial applications and possibly unpredictable changes in flow behaviors within the conveying pipelines. Depending on the system geometry, gas velocities, and material properties of the solid particles to be transported, such transportation processes can take place in different modes, usually referred to as dense or dilute-phase conveying. The former involves transportation of the solids as dense clusters or slugs and is usually the preferred method for handling solids that are sensitive to abrasion as shear and collisional forces arising within the solid material are generally lower. In comparison, the latter mode, where particles are dispersed as a suspension in the gas, is known to be a more stable mode, with lower fluctuations and excursions in gas pressures.

Numerical modeling of pneumatic conveying and other gas-solid systems plays an important role in improving our understanding of such systems. One of the commonly used approaches to pneumatic conveying modeling is the Eulerian/Lagrangian method, where particles are tracked in a Lagrangian frame of reference either individually or as groups with identical properties known as parcels.[1,2] An alternative approach has been computational fluid dynamics (CFD), with two-fluid continuum models to represent the gas and solid phases as two interpenetrating continua.[3] Further, the technique of particle dynamics simulation has also been widely used for investigations of granular and gas-solid systems. In particular, the discrete element method (DEM), originally developed by Cundall and Strack[4] for describing the mechanical behavior of assemblies of discs and spheres, has been successfully applied by many research workers in various areas of engineering interests. Tsuji et al.[5] carried out numerical simulations of horizontal pneumatic conveying of solid particles using DEM and showed that particles moved in the form of plugs in the conveying pipe. Several research workers have also applied the approach of combining DEM with CFD to the simulation of two-dimensional fluidized beds.[6-10] Li and Mason[11] used the same approach to model heat transfer between gas, solid particles, and pipe wall in a pneumatic conveying system. Han et al.[12] simulated the flow of salt particles through a dilute phase pneumatic conveying system to predict particle attrition and breakage.

An understanding of the differences in physics between the various flow regimes found in pneumatic conveying of granular material may be important to actual industrial or commercial applications with regards to the optimality of operation, ease of control, and extent of damage inflicted on the solid particles as well as the conveying lines. Despite the large amount of work reported on gas-solid systems, there have been relatively fewer attempts at modeling the various flow regimes in vertical and horizontal pneumatic conveying systems. The ability to predict the flow behaviors of both gas and solid phases during a typical pneumatic conveying operation or the modes in which the transportation would take place remains limited. As such, the objective of this study is to apply the technique of combining DEM with CFD to the numerical simulation of pneumatic conveying of granular material in both vertical and horizontal pipes. The emphasis has been on reproducing computationally the different types of solid flow patterns and behaviors observed experimentally under different operating conditions. In the following sections of this paper, the DEM and CFD models used and their methods of implementation will be described, and simulation results obtained will be compared with experimental observations reported in the literature.

Mathematical Model

Discrete element method

The translational and rotational motions of individual solid particles are governed by Newton's laws of motion:

$$m_i \frac{d\mathbf{v}_i}{dt} = \sum_{j=1}^{N} (\mathbf{f}_{c,ij} + \mathbf{f}_{d,ij}) + m_i\mathbf{g} + \mathbf{f}_{f,i} \tag{1}$$

$$I_i \frac{d\boldsymbol{\omega}_i}{dt} = \sum_{j=1}^{N} \mathbf{T}_{ij} \tag{2}$$

where m_i and $\mathbf{v}_i$ are the mass and velocity of particle i, N is the number of particles in contact with this particle, $\mathbf{f}_{c,ij}$ and $\mathbf{f}_{d,ij}$ are the contact and viscous contact damping forces, respectively, $\mathbf{f}_{f,i}$ is the fluid drag force due to an interstitial fluid, I_i is the moment of inertia of particle i, ω_i is its angular velocity, and $\mathbf{T}_{ij}$ is the torque arising from contact forces, which will cause the particle to rotate.

Contact and viscous contact damping forces have to be calculated using force-displacement models that relate such forces to the relative positions, velocities, and angular velocities of the colliding particles. In the present work, the linear force-displacement model was implemented according to the following equations:

$$\mathbf{f}_{cn,ij} = -\kappa_{n,i}\boldsymbol{\delta}_{n,ij} \tag{3}$$

$$\mathbf{f}_{ct,ij} = -\kappa_{t,i}\boldsymbol{\delta}_{t,ij} \tag{4}$$

$$\mathbf{f}_{dn,ij} = -\eta_{n,i}(\mathbf{v}_r \cdot \mathbf{n}_i)\mathbf{n}_i \tag{5}$$

$$\mathbf{f}_{dt,ij} = -\eta_{t,i}\{(\mathbf{v}_r \cdot \mathbf{t}_i)\mathbf{t}_i + (\boldsymbol{\omega}_i \times \mathbf{R}_i - \boldsymbol{\omega}_j \times \mathbf{R}_j)\} \tag{6}$$

where $\mathbf{f}_{cn,ij}$, $\mathbf{f}_{dn,ij}$, and $\mathbf{f}_{ct,ij}$, $\mathbf{f}_{dt,ij}$ are the normal and tangential components of the contact and viscous contact damping forces, respectively, $\kappa_{n,i}$, $\delta_{n,ij}$, $\mathbf{n}_i$, and $\eta_{n,i}$ and $\kappa_{t,i}$, $\delta_{t,ij}$, $\mathbf{t}_i$, and $\eta_{t,i}$ are the spring constants, displacements between particles, unit vectors, and viscous contact damping coefficients in the normal and tangential directions, respectively, $\mathbf{v}_r$ is the relative velocity between particles, and $\mathbf{R}_i$ and $\mathbf{R}_j$ are the radius vector (from particle center to a contact point) for particles i and j, respectively. If $|\mathbf{f}_{ct,ij}| > |\mathbf{f}_{cn,ij}|\tan\phi + c$ then "slippage" between the two contacting surfaces is simulated by a Coulomb-type friction law, $|\mathbf{f}_{ct,ij}| = |\mathbf{f}_{cn,ij}|\tan\phi + c$ where $\tan\phi$ is analogous to the coefficient of friction and c is a measure of cohesion between the two contacting surfaces.

Fluid drag force

In a multiphase system, such as the gas-solid pneumatic conveying system considered in this study, interactions between the two phases take the form of fluid drag forces on the solid particles exerted by the interstitial fluid and arise from velocity differences between the two phases. In this study, the model due to Di Felice,[13] which is applicable over a wide range of particle Reynolds numbers, was used for evaluating the fluid drag force term in Eq. 1. Following Xu et al.,[14] the modified equations in this model are shown as follows:

$$\mathbf{f}_{f,i} = \mathbf{f}_{f0,i}\varepsilon_i^{-(\chi+1)} \tag{7}$$

$$\mathbf{f}_{f0,i} = 0.5c_{d0,i}\rho_f\pi R_i^2\varepsilon_i^2|\mathbf{u}_i - \mathbf{v}_i|(\mathbf{u}_i - \mathbf{v}_i) \tag{8}$$

$$\chi = 3.7 - 0.65\ \exp\left[-\frac{(1.5 - \log_{10}\mathrm{Re}_{p,i})^2}{2}\right] \tag{9}$$

$$c_{d0,i} = \left(0.63 + \frac{4.8}{\mathrm{Re}_{p,i}^{0.5}}\right)^2 \tag{10}$$

$$\mathrm{Re}_{p,i} = \frac{2\rho_f R_i\varepsilon_i|\mathbf{u}_i - \mathbf{v}_i|}{\mu_f} \tag{11}$$

where $\mathbf{f}_{f0,i}$ is the fluid drag force on particle i in the absence of other particles, χ is an empirical parameter, ε_i is the local average porosity in the vicinity of particle i, $c_{d0,i}$ is the drag coefficient, $\mathrm{Re}_{p,i}$ is the Reynolds number based on particle diameter, ρ_f is the fluid density, μ_f is the fluid viscosity, and $\mathbf{u}_i$ is the fluid velocity of the computational cell in which particle i is located.

Rolling friction model

It is well recognized that rolling against a contacting surface is a common state of motion of solid particles, in addition to pure translational or rotational motions. This arises when the translational velocity of a particle is exactly equal but opposite in direction to the tangential velocity due to rotation at the point of contact such as to give rise to a "no-slip" condition between the two surfaces. In the presence of only sliding frictional effects simulated by the Coulomb friction law, a particle in such a state of motion tends to preserve its kinetic energy for unrealistically long traveling times and distances. As such, a rolling friction model, which simulates resistances against rolling motion in terms of a torque that opposes this "no-slip" rotation of a particle, may be essential for an accurate representation of such motions. Zhou et al.[15] found that implementation of such a rolling friction model in DEM is necessary for realistic simulations of particle heap formation with angles of repose comparable with experimental observations. They advocated the following angular velocity-independent rolling friction model due to Beer and Johnson[16]:

$$\mathbf{M}_i = \mu_r\mathbf{f}_{cn,ij} \tag{12}$$

where $\mathbf{M}_i$ is the torque that opposes rotation of the particle and is opposite in direction to that of its angular velocity, and μ_r is the coefficient of rolling friction. This rolling friction model was similarly incorporated into DEM in this study to ensure realistic simulations of particle motions and dynamics.

Numerical integration

The numerical procedure for particle dynamics simulation involves alternating between integration of Newton's second law and the force-displacement model. In order to enhance the numerical stability of the code, the well-known Verlet algorithm[17] commonly used in molecular dynamics simulation was used for time integration of Newton's law and evaluation of particle positions and velocities. The equations involved in this algorithm are given as follows:

$$\mathbf{x}_i(t + \Delta t) = -\mathbf{x}_i(t - \Delta t) + 2\mathbf{x}_i(t) + \frac{\mathbf{F}_i(t)}{m_i}\Delta t^2 \tag{14}$$

$$\mathbf{v}_i(t + \Delta t) = \frac{\mathbf{x}_i(t + \Delta t) - \mathbf{x}_i(t - \Delta t)}{2\Delta t} \tag{15}$$

where $\mathbf{x}_i$ is the position vector of particle i represented by Cartesian coordinates, $\mathbf{F}_i$ is the total force acting on the particle equal to the sum of all terms on the right hand side of Eq. 1, and Δt is the time step used.

Computational fluid dynamics

The motion of the continuum gas phase is governed by the Navier-Stokes equations, with an additional source term in the momentum equation to represent the reaction force acting on the fluid by the particles:

$$\frac{\partial\varepsilon}{\partial t} + \nabla\cdot(\varepsilon\mathbf{u}) = 0 \tag{16}$$

$$\frac{\partial(\rho_f\varepsilon\mathbf{u})}{\partial t} + \nabla\cdot(\rho_f\varepsilon\mathbf{u}\mathbf{u}) = -\nabla P + \nabla\cdot(\mu_f\varepsilon\nabla\mathbf{u}) + \rho_f\varepsilon\mathbf{g} - \mathbf{F} \tag{17}$$

where $\mathbf{u}$ is the velocity vector, ε is the local average porosity, P is the fluid pressure, and $\mathbf{F}$ is the source term due to fluid-particle interaction.

In the present study, the numerical solution of the Navier-Stokes equations was carried out using the first-order upwind difference scheme for discretizing the convection term, the central difference scheme for the diffusion term, and the SIMPLE method[18] for pressure prediction. The computational domain was divided into uniform grid cells, and all quantities such as velocities and pressure were assumed constant over each cell. The source term $\mathbf{F}$ for a particular computational cell was calculated by summing the fluid drag forces on all particles present within that cell:

$$\mathbf{F} = \frac{\sum_{i=1}^{n}\mathbf{f}_{f,i}}{\Delta V} \tag{18}$$

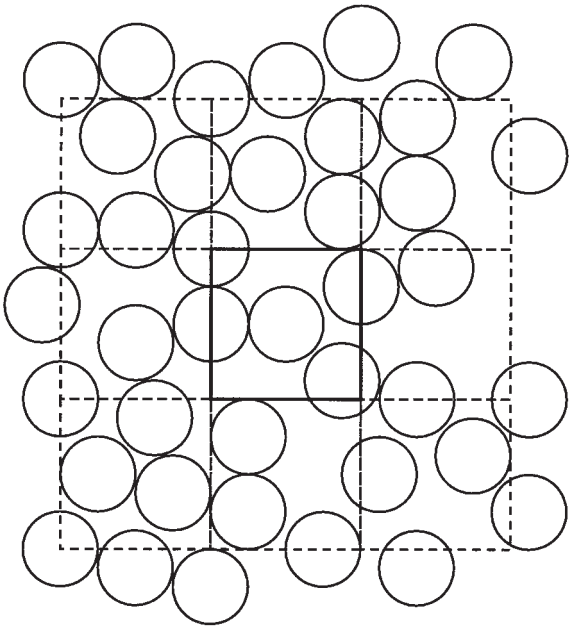

Figure 1. Computational cells used in the calculation of local porosity. The surrounding eight cells are included in the calculation of the porosity value for the central cell.

where ΔV is the volume of a computational cell and n is the number of particles present in the cell.

Porosity calculation

Fluid drag forces are strong functions of porosity values. The local average porosity ε_i in the neighborhood of a particle as applied in Eq. 7 of the Di Felice model is defined as the porosity value within the computational cell in which the particle is residing. This is normally calculated by taking 1.0 minus the ratio of the total volume of all particles found within the computational cell to that of the cell.[8] Two approaches are used to calculate the porosity of a computational cell. First, a particle is usually defined to be completely in a computational cell as long as its center is located within the space enclosed by the boundaries of the cell, while errors arising from particles lying only partially within a cell have largely been neglected.[5] Secondly, only the partial volumes of particles that are included in a computational cell are taken into account when the particles are located over the cell boundaries.[7,9] Obviously, the second approach is more accurate and should be used. On the other hand, the first approach is also attractive because it can reduce the computational effort involved. The first approach was employed in the present work. However, it has been modified in order to meet the need for accuracy and efficiency, as described below.

In CFD, the sizes of computational cells have to be small for fine resolution of the fluid flow pattern. On the other hand, as illustrated in Figure 1, a small computational cell has the effect of magnifying the abovementioned errors associated with porosity calculation as the proportion of particle volumes that lie outside the cell but that have been assumed to be within the cell is large. To resolve this issue in a computationally efficient manner, a modification to the conventional method of porosity calculation is proposed in this study. The size of computational cells used is kept minimal but larger than the characteristic size of a single particle, in accord with the idea of local averaging for all fluid properties. However, the local average porosity in the vicinity of a particle ε_i is calculated from the ratio of volumes of all particles located within the computational cell under consideration as well as those located in the immediate neighboring eight cells (Figure 1) to the total volume of these nine cells (Eq. 19). This allows the use of small computational cells to ensure accurate CFD calculations without compromising the accuracies of porosity estimations at the same time.

$$\varepsilon = 1 - \frac{\sum_{i=1}^{k} V_i}{9\Delta V} \tag{19}$$

where k is the total number of particles in nine computational cells for a two-dimensional system and V_i is the volume of particle i. In both Eqs. 18 and 19, the volume of a computational cell ΔV is calculated based on a pseudo-three-dimensional geometry assumption whereby the "thickness" of the computational domain in the spanwise direction is assumed to be equal to the particle diameter used.

Simulation Conditions

The geometry of the pneumatic conveying system and type of particles used in the present simulations were based on the experimental work of Rao et al.[19] and Zhu et al.[20] (Table 1) so that a meaningful comparison between the simulation and experimental outputs can be made. The gas velocities considered in this study were in the ranges 14 m s^{-1}-24 m s^{-1} and 10 m s^{-1}-30 m s^{-1} for the vertical and horizontal pneumatic conveying simulations, respectively, because these would include all the flow regimes observed via electrical capacitance tomography measurements by Rao et al.[19] and Zhu et al.[20] for the two systems. The numbers of particles used were 500, 1000, 1500, and 2000, corresponding to overall solid concentrations α, of 0.08, 0.16, 0.24, and 0.32, respectively, where α is defined as the overall volume fraction of particles divided by the volume fraction of particles at maximum packing, which is generally taken to be 0.64. The equivalent coefficient of restitution represented by the viscous contact damping coefficient selected for the present study was found by conducting a

Table 1. Material Properties and System Parameters

Shape of particles	Spherical
Type of particles	Polypropylene
Number of particles	500, 1000, 1500, 2000
Particle diameter, d	2.8×10^{-3} m
Particle density, ρ_p	1123 kg m^{-3}
Spring constant in force model, κ	5.0×10^{3} N m^{-1}
Viscous contact damping coefficient, η	0.35
Coefficient of restitution	0.1
Coefficient of friction	0.3
Cohesion, c	0.0
Coefficient of rolling friction, μ_r	5.0×10^{-5} m
Gas density, ρ_f	1.205 kg m^{-3}
Gas viscosity, μ_f	1.8×10^{-5} N s m^{-2}
Pipe diameter	0.04 m
Pipe length	1.0 m
Computational cell size	4 mm × 4 mm
Simulation time step, Δt	10^{-7} s

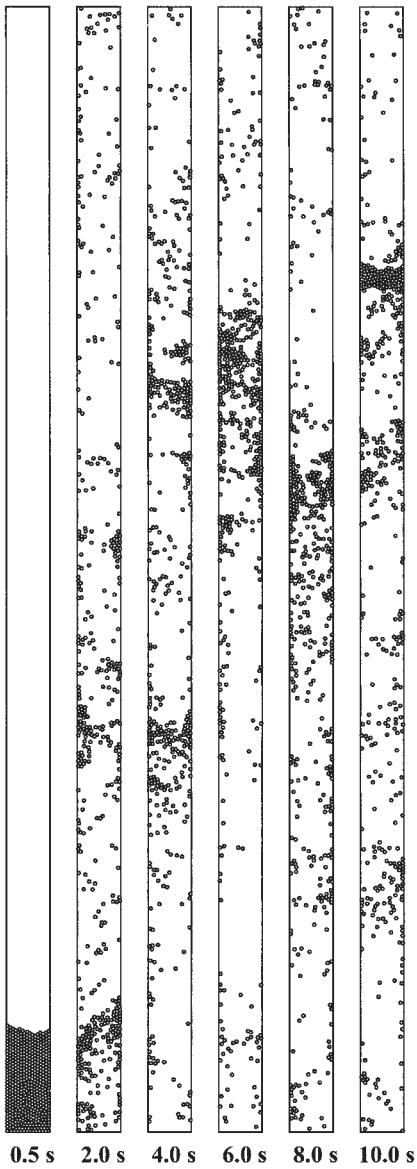

Figure 2. Vertical pneumatic conveying in the dispersed flow regime with α = 0.08 (500 particles) and gas velocity 14 m s^{-1}.

numerical experiment similar to that used by Xu and Yu.[7] A single particle was simulated to fall from rest under the effects of gravity and rebound from a flat surface. The coefficient of restitution was then given by $\sqrt{(h/h_o)}$ where h_o and h are the maximum heights of the particle above the surface before and after the collision, respectively. The value obtained was insensitive to h_o and a value of 1 m was used for this quantity for all subsequent calibration of the viscous contact damping coefficient to the coefficient of restitution. Without loss of generality, the same values of the coefficients of friction and restitution as shown in Table 1 were used for both particle-particle and particle-wall interactions. The flow patterns from the numerical simulations were then compared qualitatively with the experimental observations of Rao et al.[19] and Zhu et al.[20]

In all simulations performed, particles were first allowed to settle freely under gravity for 0.5 s and form a packing at the "bottom" of a vertical pipe or a heap in a horizontal pipe before gas flow was initiated. Periodic boundary conditions were applied to the solid phase to simulate an open flow system, while a uniform gas velocity profile was maintained at the inlet. Particles that were carried out of the conveying pipe by the flowing gas were simulated to re-enter from the inlet of the pipe with the same velocities and radial positions. The main advantage of this method was the possibility of simulating a very long conveying pipe using a significantly smaller computational domain, which leads to more efficient utilization of computing resources.

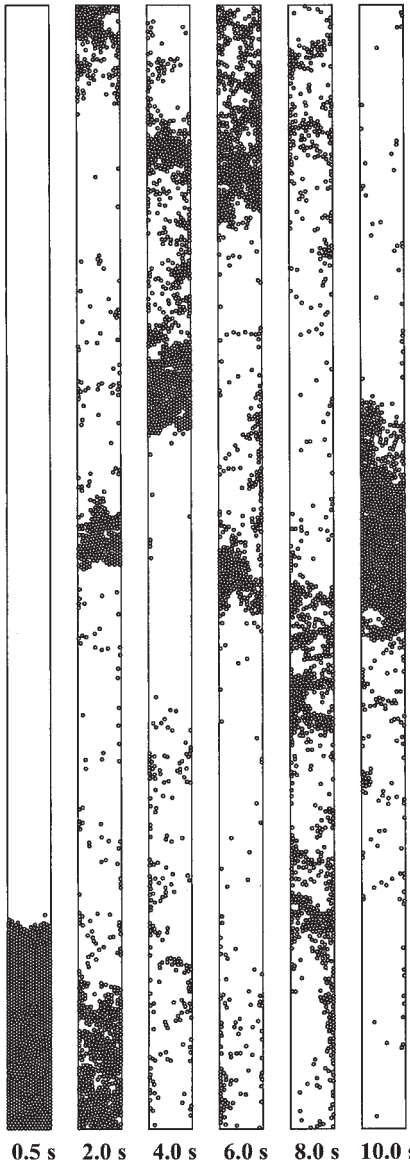

Figure 3. Vertical pneumatic conveying showing transition between the dispersed and plug flow regimes with α = 0.16 (1000 particles) and gas velocity 14 m s^{-1}.

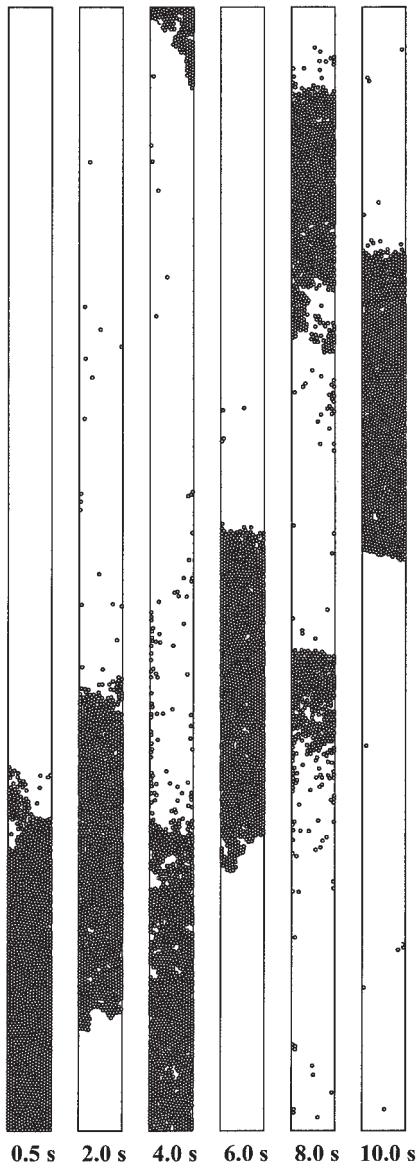

Figure 4. Vertical pneumatic conveying in the plug flow regime with $\alpha = 0.24$ (1500 particles) and gas velocity 14 m s^{-1}.

Results and Discussion

Vertical pneumatic conveying

The combined CFD-DEM model described in this paper was first used for the numerical simulation of pneumatic conveying of granular material in a vertical pipe. From the simulation outputs obtained, two distinct types of flow regimes could be identified. Figure 2 shows the case where the solid concentration was 0.08 and the gas velocity was 14 m s^{-1}. Particles are seen to be distributed throughout the entire length of the pipe. This kind of flow pattern, known generally as dispersed flow, persisted for the 10 s of physical time simulated, during which particles cycled through the pipe numerous times. In contrast, Figure 3 shows the case where $\alpha = 0.16$ at the same gas velocity. There seems to be a tendency for particles to cluster together and be re-dispersed again into a homogeneous suspension intermittently. This indicates that the operating conditions applied may correspond to an unstable flow regime that oscillates between that of dispersed flow and plug flow continuously. When α was increased further to 0.24 and 0.32, the clusters of particles formed during the transportation process remained stable throughout the entire simulation time. Figures 4 and 5 show that particles in these cases move in the form of a single large plug along the conveying pipe. Generally, it is known from previous experimental work reported in the literature that the dispersed flow regime is usually dominant at high gas velocities and low solid concentrations, while the plug flow regime is observed otherwise.[20] At a gas velocity of 24 m s^{-1}, the simulation outputs for $\alpha = 0.08$ and 0.16 presented in Figures 6 and 7, respectively, show that both cases exhibit dispersed flow, while those using $\alpha = 0.24$ and 0.32 exhibited plug flow (Figures 8 and 9). The simulations with $\alpha = 0.08$

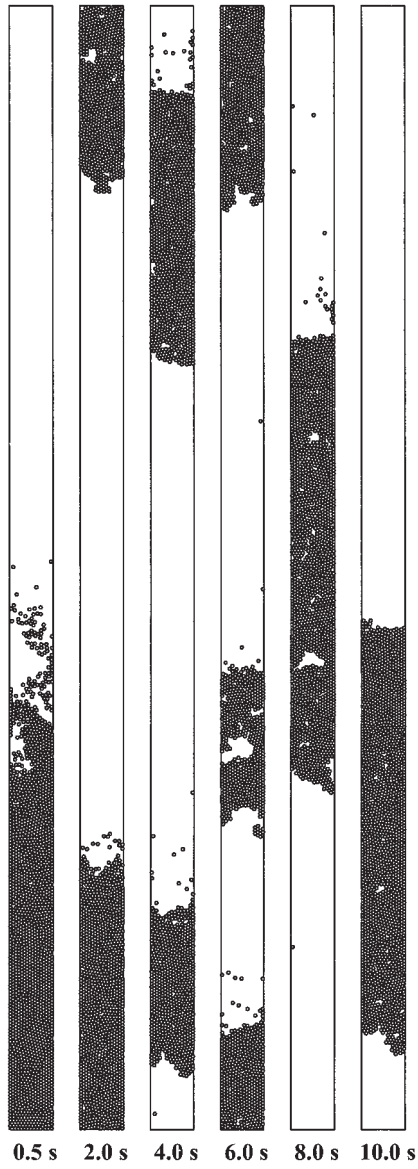

Figure 5. Vertical pneumatic conveying in the plug flow regime with $\alpha = 0.32$ (2000 particles) and gas velocity 14 m s^{-1}.

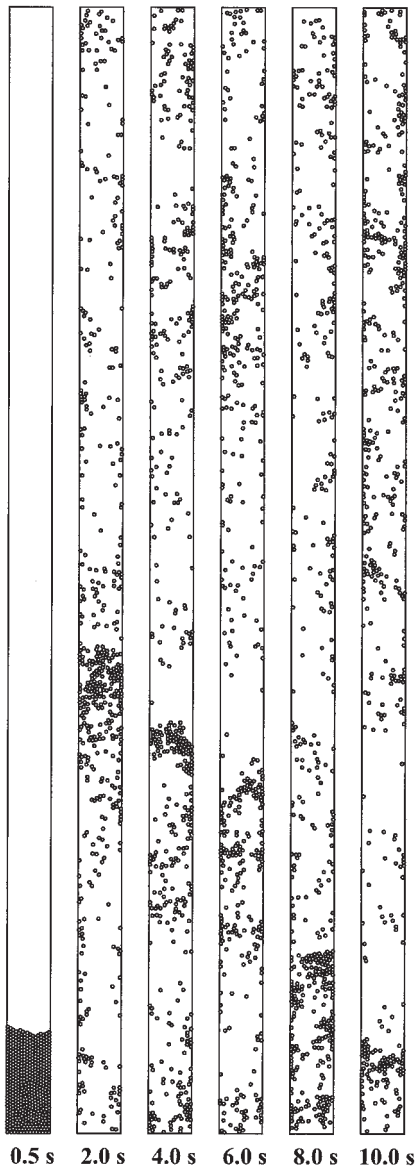

Figure 6. Vertical pneumatic conveying in the dispersed flow regime with $\alpha = 0.08$ (500 particles) and gas velocity 24 m s^{-1}.

representing vertical pneumatic conveying at a relatively low solid concentration verified the general experimental observation that the dominant flow regime encountered under such conditions was dispersed flow even at the lowest gas velocity of 14 m s^{-1} considered. The case with $\alpha = 0.16$ has shown a transition from an unstable plug flow regime to a dispersed flow regime when the gas velocity was increased from 14 m s^{-1} to 24 m s^{-1}. On the other hand, at high solid concentrations of 0.24 and 0.32 represented by the use of 1500 and 2000 particles, respectively, in the simulation, the plug flow regime remained dominant even up to the gas velocity of 24 m s^{-1}. These general observations and trends with respect to the types of flow regimes observed under different operating conditions and their transitions agree well with the experimental observations of Zhu et al.[20] This is also the first successful direct simulation of these two important flow regimes frequently observed in pneumatic conveying in vertical pipes, and the procedure used involved varying the gas velocity and solid concentration only, much like what would be done in a physical experiment. Other flow regimes that have been observed experimentally, such as the moving annular capsules described by Zhu et al.[20] and ring or half-ring flow regimes observed by Yao et al.[21], may have arisen due to the effects of electrostatics, and the present study may be a good starting point for further explorations into such effects in pneumatic conveying systems.

The solid concentration profiles for both flow regimes were obtained by dividing the space in the conveying pipe into long strips parallel to the length of the pipe and calculating the solid concentration within each strip. It was observed that this spatially averaged solid concentration profile became invariant with time after a sufficiently long simulation time, indicating the attainment of a fully developed flow state. The time re-

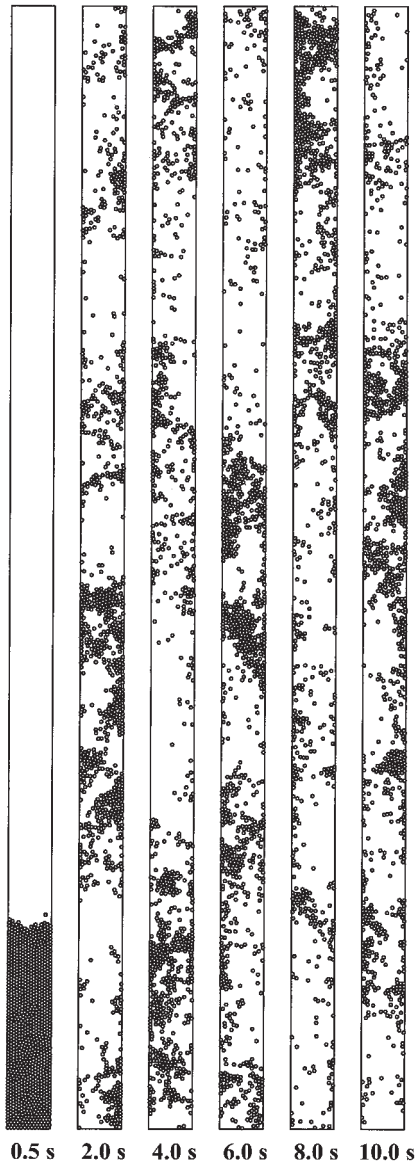

Figure 7. Vertical pneumatic conveying in the dispersed flow regime with $\alpha = 0.16$ (1,000 particles) and gas velocity 24 m s^{-1}.

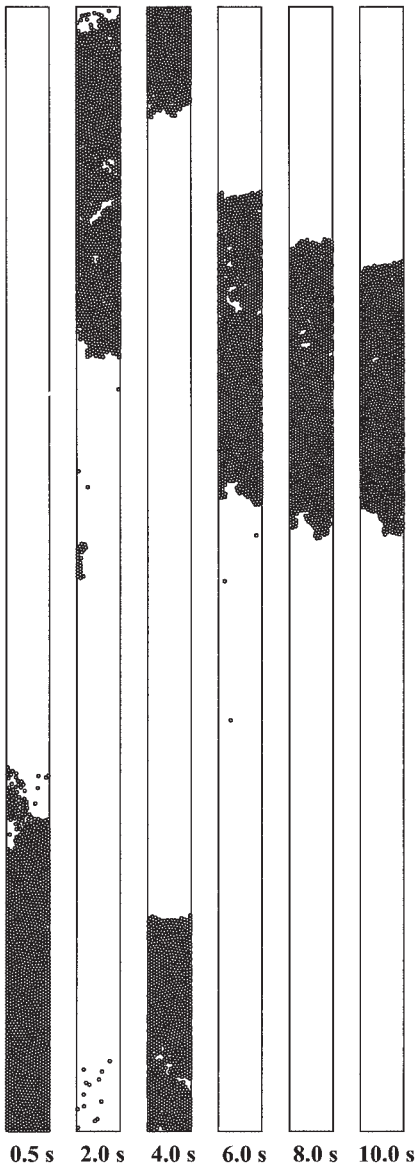

Figure 8. Vertical pneumatic conveying in the plug flow regime with $\alpha = 0.24$ (1,500 particles) and gas velocity 24 m s^{-1}.

quired also corresponded to that required for the solid flow rate to reach a steady value. This latter point would be elaborated in a later section. Figures 10 and 11 show the solid concentration profile for the dispersed ($\alpha = 0.08$) and plug ($\alpha = 0.32$) flow regimes at various gas velocities, respectively. It may be observed that, contrary to the name of the regime and the qualitative observations that can be made from the instantaneous snapshots of the simulation, the solid concentration profile for dispersed flow shows a symmetrical but non-uniform distribution, with higher solid concentrations near the walls and a minimum near the center of the pipe. This may be due to the effects of inelastic collisions with the walls, which leave particles lying in the vicinity of the walls. On the other hand, the solid concentration profile for the plug flow regime is uniform and flat across the section of the pipe. This is due to the fact that particles in such a regime are closely packed together into a single large plug that moves much like a rigid body along the conveying pipe. For each of these regimes studied, the solid concentration profiles do not seem to be significantly affected by the actual velocity of the gas used.

Horizontal pneumatic conveying

The simulation outputs for horizontal pneumatic conveying showed a few other types of flow patterns in addition to those observed in vertical pneumatic conveying. These arise mainly due to gravitational effects, which cause particles to settle towards the bottom wall of the conveying pipe. At a low solid concentration of 0.08 represented by 500 particles and conveying gas velocity of 10 m s^{-1}, the flow pattern observed in Figure 12 resembles that of dispersed flow in vertical pneumatic conveying but, due to the effects of gravitational settling

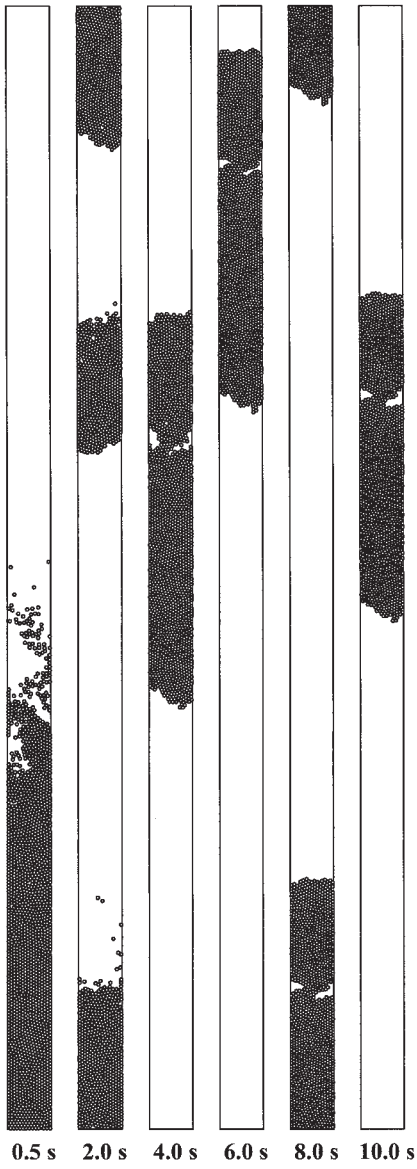

Figure 9. Vertical pneumatic conveying in the plug flow regime with $\alpha = 0.32$ (2,000 particles) and gas velocity 24 m s^{-1}.

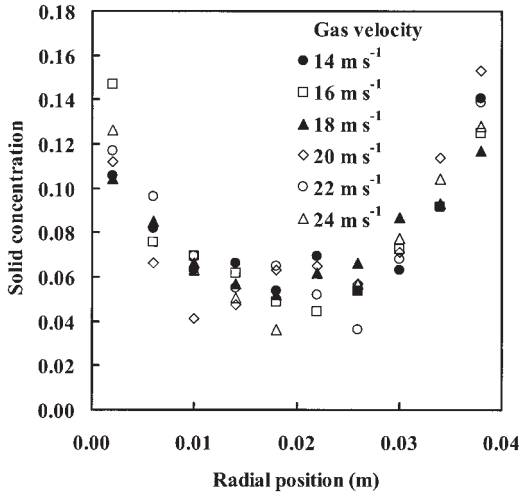

Figure 10. Solid concentration profile for the dispersed flow regime in vertical pneumatic conveying (α = 0.08) at various gas velocities showing symmetry and minimum near the pipe center.

as mentioned, a thin layer of particles is formed along the lower pipe wall. There exists a gradient in the concentration of particles in the radial direction, with higher concentration of particles near the lower pipe wall and vice versa. This flow regime was also observed under similar operating conditions experimentally and is known as the stratified flow regime.[19] With $\alpha = 0.16$, it can be seen in Figure 13 that the previously observed thin settled layer of particles has become larger clusters, which move along the lower wall by traction. The individual clusters do not seem to have a tendency to combine together nor be dispersed into suspension but remain quite stable throughout the entire simulation time. A large portion of the particles is still transported in suspension above these moving clusters. Following the experimental work of Rao et al.,[19], this is referred to as the moving dunes flow regime.

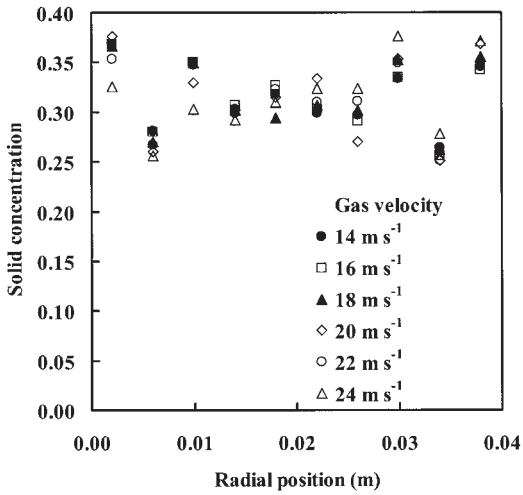

Figure 11. Solid concentration profile for the plug flow regime in vertical pneumatic conveying (α = 0.32) at various gas velocities showing a flat distribution.

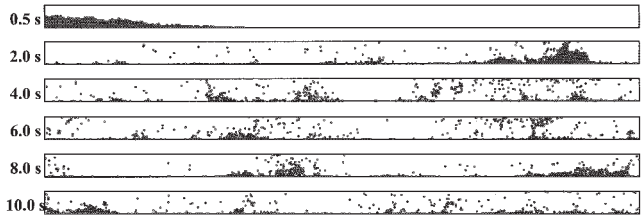

Figure 12. Horizontal pneumatic conveying in the stratified flow regime with α = 0.08 (500 particles) and gas velocity 10 m s^{-1}.

In contrast, at the highest solid concentrations of 0.24 and 0.32 considered in the present simulation using 1500 and 2000 particles, respectively, particles tend to be transported in the form of a single large cluster reminiscent of plug flow in vertical pneumatic conveying (Figures 14 and 15). This may be a result of clustering of multiple adjacent moving dunes to form a stable large plug that spans the entire cross-section of the conveying pipe. This kind of flow pattern was similarly observed in physical experiments done at high solid concentrations and low gas velocities and was called the slug flow regime. When the gas velocity was increased to 30 m s^{-1} in the present simulation, it can be seen in Figures 16 and 17 that the original stratified and moving dunes flow regimes observed with $\alpha = 0.08$ and 0.16, respectively, have transformed into a homogeneous flow pattern. Most of the particles are now transported in suspension along the pipe and seem to be distributed throughout the entire length of the conveying line. The relative effect of gravitational settling is lower due to the higher conveying velocity, resulting in minimal non-homogeneity in particle distribution. However, cases where $\alpha = 0.24$ and 0.32 showed that the slug flow regime remained as the dominant regime at these high solid concentrations up to the gas velocity of 30 m s^{-1}. As with the vertical pneumatic conveying simulations, these different flow regimes do not seem to have been reproduced computationally previously. Tsuji et al.[5] simulated a type of slug flow in a horizontal pipe that they referred to as plug flow. However, other types of flow regimes, and in particular the moving dunes, have only been observed in physical experiments so far. It may not even be possible in principle to reproduce this type of flow pattern computationally using two-fluid continuum models.

The solid concentration profiles for two representative regimes in horizontal pneumatic conveying, stratified flow (α = 0.08) and slug flow (α = 0.32), were similarly computed for a quantitative comparison of the effects of gravitational settling mentioned earlier on the resulting solid distribution. Figure 18

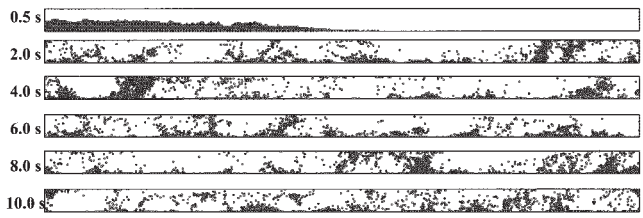

Figure 13. Horizontal pneumatic conveying in the moving dune flow regime with α = 0.16 (1,000 particles) and gas velocity 10 m s^{-1}.

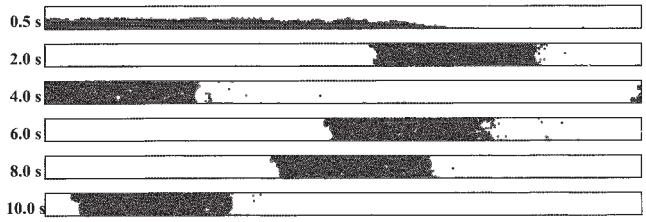

Figure 14. Horizontal pneumatic conveying in the slug flow regime with $\alpha = 0.24$ (1,500 particles) and gas velocity 10 m s^{-1}.

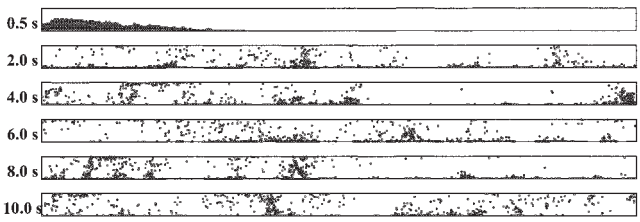

Figure 16. Horizontal pneumatic conveying in the homogeneous flow regime with $\alpha = 0.08$ (500 particles) and gas velocity 30 m s^{-1}.

shows quantitatively that the solid concentration is higher near the bottom wall of the horizontal pipe when particles are conveyed in the stratified flow regime, corresponding to the qualitative observations made from the simulation snapshots seen previously. By comparison with the solid concentration profile for dispersed flow in vertical pneumatic conveying, the effect of gravitational settling has caused the profile to change from a symmetrical distribution to an unsymmetrical one. In contrast, the solid concentration profile for slug flow (Figure 19) is seen to be very similar to that for plug flow in vertical pneumatic conveying. This fits well with the fact that particles are carried in the form of a single large plug in both cases. When this occurs in a horizontal pipe, the effect of gravity does not alter the solid concentration profile to any significant extent. As with the previous cases for vertical pneumatic conveying, the solid concentration profiles for each type of flow regime at different gas velocities are similar for the range of velocities investigated.

Phase diagrams

The different flow regimes in vertical and horizontal pneumatic conveying arising from the use of different operating conditions can be represented in the form of phase diagrams, as shown in Figures 20 and 21, respectively. Dashed lines in the figures separate approximately the regions representing different flow regimes, while dashed circles enclose regions where transition between two adjacent flow regimes might be taking place. In vertical pneumatic conveying, the dispersed flow regime is dominant at high gas velocities and low solid concentrations, while the plug flow regime is dominant otherwise (Figure 20). This is also generally true for horizontal pneumatic conveying, except at low gas velocities and solid concentrations where the effects of gravitational settling of particles result in the formation of the moving dunes and stratified flow regimes (Figure 21). Intermediate values of gas velocities, where transitions between the moving dunes and homogeneous flow regimes (MD/H) and between the stratified and homogeneous flow regimes (S/H) are similarly approximated, and shown by regions enclosed within the dashed circles in Figure 21.

Solid flow rate

Figures 22 and 23 show, respectively, the transient development of the solid flow rates in vertical and horizontal pneumatic conveying at various gas velocities and for the case of $\alpha = 0.16$. The flow rates increase sharply from an initial value of zero at time 0.5 s when gas flow is initiated and reach a steady value after about 3 s of physical time. Flow rate profiles at other solid concentrations are similar to those presented and are not shown for the sake of brevity. As mentioned in an earlier section, the attainment of a time-invariant solid concentration profile corresponded with that of a steady state defined by a constant solid flow rate. In view of this point and in consideration of the high computational demands of the present study (each simulation case shown earlier requires between 1 and 3 weeks of computer time on a Linux cluster with Pentium Xeon 3.06 GHz processors), it was deemed justifiable to simulate for a relatively short physical time of 10 s in each case before quantitative characterization of each flow regime was carried out.

As may be seen from Figure 22 for vertical pneumatic conveying, the case where the gas velocity was equal to 15 m s^{-1} resulted in a lower solid flow rate than that at 14 m s^{-1}. This was attributed previously to an unstable flow regime occurring near the transition between dispersed and plug flow. The apparent hysteresis in the solid flow rate was investigated further by tracking the variation of solid flow rate with respect to time as the gas velocity was increased (or decreased) from an initially low value of 14 m s^{-1} (or correspondingly high value of 18 m s^{-1}) to a high value of 18 m s^{-1} (or low value of 14 m

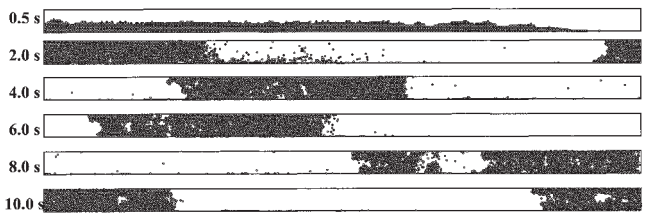

Figure 15. Horizontal pneumatic conveying in the slug flow regime with $\alpha = 0.32$ (2,000 particles) and gas velocity 10 m s^{-1}.

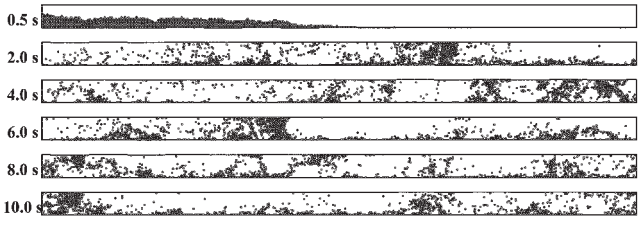

Figure 17. Horizontal pneumatic conveying in the homogeneous flow regime with $\alpha = 0.16$ (1,000 particles) and gas velocity 30 m s^{-1}.

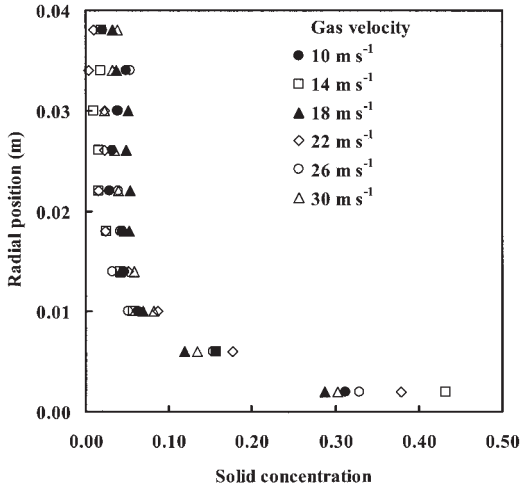

Figure 18. Solid concentration profile for the stratified flow regime in horizontal pneumatic conveying (α = 0.08) at various gas velocities showing non-symmetry and higher solid concentration near the bottom wall.

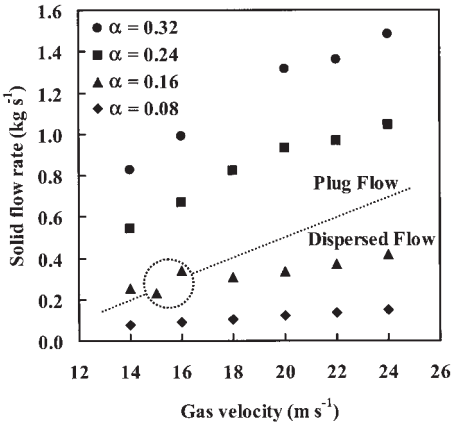

Figure 20. Phase diagram for vertical pneumatic conveying.

Dashed lines separate approximately regions representing different flow regimes, while dashed circles enclose regions where transition between two adjacent flow regimes might be taking place. The dispersed flow regime is dominant at high gas velocities and low solid concentrations, while the plug flow regime is dominant otherwise.

s^{-1}) past the point where transition was expected to occur. The system was first allowed to reach a steady state with the initial gas velocity used in the usual manner before changes in gas velocity were implemented in the form of step increases (or decreases) of magnitude 0.5 m s^{-1} at one second intervals. Figure 24 shows that the time variations of solid flow rates for the two cases described exhibit hysteresis. The start (and end) point of one graph does not correspond to the end (and start) point of the other in terms of solid flow rate values obtained. As such, in the range of gas velocity values where hysteresis occurs, there might be more than one solid flow rate value that the system can undertake, and this may be the reason for the previously observed anomalous values in the phase diagram of Figure 20 and steady state solid flow rates in Figure 22. In general, transitions between flow regimes in pneumatic conveying systems seem to be complex processes that are path dependent and sensitive to the specific operating conditions used. They may be the subject of a more detailed study in the future.

Sensitivity analyses

The parameters deemed to be important in any typical discrete element simulation include the spring constant, viscous contact damping coefficient, and coefficient of friction used in the force-displacement model. The spring constant determines the stiffness of the spring used in modeling inter-particle or

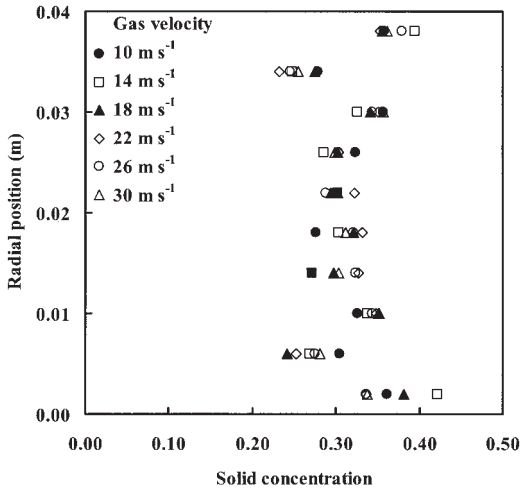

Figure 19. Solid concentration profile for the slug flow regime in horizontal pneumatic conveying (α = 0.32) at various gas velocities showing a flat distribution (order of coordinates is different from Figure 11 to aid in visualization).

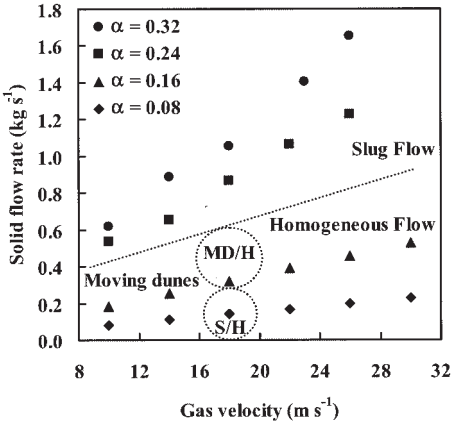

Figure 21. Phase diagram for horizontal pneumatic conveying.

Homogeneous flow is dominant at high gas velocities and low solid concentrations. The effects of gravitational settling result in the formation of the moving dunes and stratified flow regimes at low gas velocities and solid concentrations. MD/H and S/H denote transitions between moving dunes and homogeneous flow and between stratified and homogeneous flow, respectively.

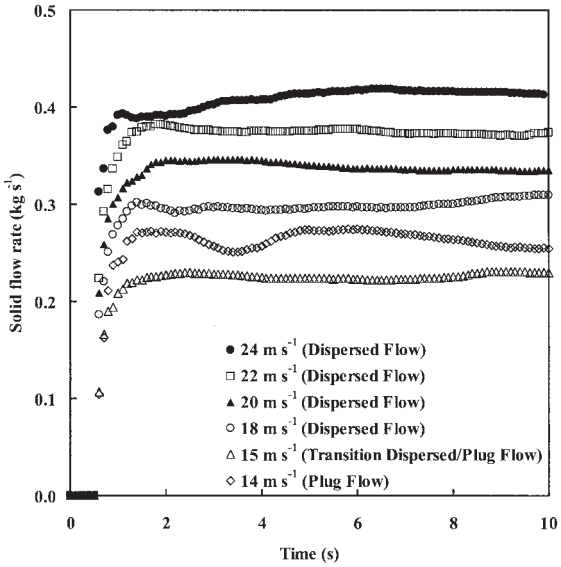

Figure 22. Transient development of solid flow rates at various gas velocities in vertical pneumatic conveying.

Steady state is reached after about 3 s of physical time. Each simulation is performed for 10 s before quantitative characterization of each flow regime is carried out.

particle-wall collisions and so is an indication of the hardness of the colliding entities. On the other hand, the viscous contact damping coefficient determines the amount of energy lost during a collision in analogy with the way energy is damped in a dashpot and so affects the elasticity of collisions. Finally, the coefficient of friction is a representation of surface roughness for both particles and pipe walls. Although these parameters

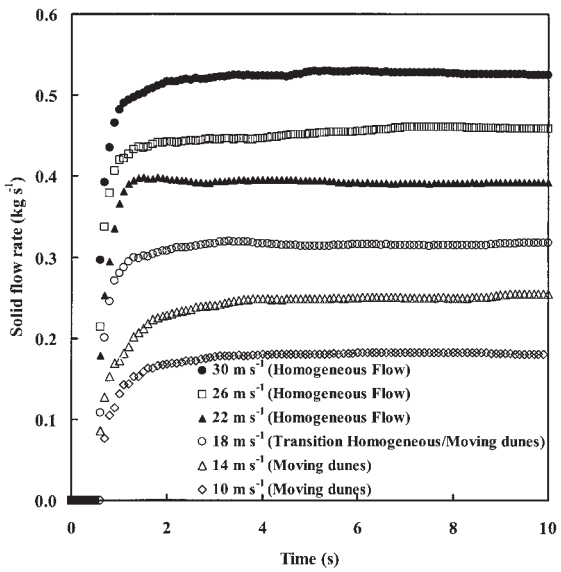

Figure 23. Transient development of solid flow rates at various gas velocities in horizontal pneumatic conveying.

Steady state is reached after about 3 s of physical time. Each simulation is performed for 10 s before quantitative characterization of each flow regime is carried out.

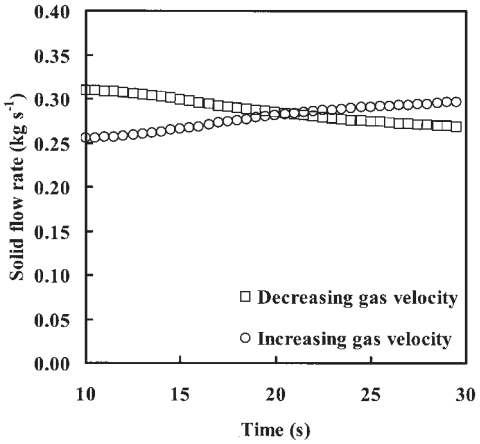

Figure 24. Time variation of solid flow rate in vertical pneumatic conveying for varying gas velocities.

Hysteresis occurs in the range of gas velocity values where transition between two flow regimes may be taking place.

are related to physical and material properties of the particles and pipe walls for the specific system considered here, their values are not readily available in the literature. As such, the investigation of the influence of these parameters on the qualitative features of flow patterns obtained was deemed an important component of this study, and this was carried out through simple sensitivity analyses during the initial phase of this work. It was found that the simulation results obtained in terms of the solid flow pattern at different gas velocities were insensitive to the three parameters in the range of values 10^3-10^4 N m^{-1} for the spring constant, 0.20-0.35 for the viscous contact damping coefficient (equivalently, 0.3-0.1 for the coefficient of restitution), and 0.2-0.8 for the coefficient of friction. Thus, the specific values selected for subsequent detailed simulation studies as presented in Table 1 previously were assumed to have negligible effects on the formation of the various flow regimes described earlier, and these would have been the results of complex gas-solid interactions reproduced realistically with the combined CFD-DEM model developed in this study.

The quantitative influences of the coefficient of friction and viscous contact damping coefficient were investigated by comparing the steady state solid flow rates obtained at different values of these parameters. The system geometry and operating conditions, which were kept constant throughout this analysis, included the vertical pipe configuration, gas velocity of 14 m s^{-1}, and overall solid concentration $\alpha = 0.16$ (1000 particles). Table 2 shows that the coefficient of friction has a marginal influence on the steady state solid flow rate. As the surface roughness of the particles and walls increases, the solid flow

Table 2. Effect of Coefficient of Friction on Solid Flow Rate

Coefficient of Friction	Solid Flow Rate (kg s^{-1})
0.3	0.255
0.4	0.238
0.5	0.237
0.6	0.237
0.8	0.225

Table 3. Effect of Coefficient of Restitution on Solid Flow Rate

Coefficient of Restitution	Solid Flow Rate (kg s^{-1})
0.1	0.255
0.2	0.211
0.3	0.208
1.0	0.226

rate achieved decreases monotonically but only marginally. As mentioned earlier, the flow regimes were qualitatively similar in the range of values shown. In contrast, Table 3 shows that the coefficient of restitution does not seem to have a direct effect on the solid flow rate within the range of values investigated. The flow patterns obtained are also insensitive to this parameter in the range 0.1-0.3. An example of a flow pattern obtained with a parameter value outside this range is shown in Figure 25. Other conditions, such as gas velocity of 14 m s^{-1} and $\alpha = 0.16$ (1000 particles), were kept identical to those used for simulating the plug flow regime shown in Figure 3. Figures 25a and b show qualitatively the flow patterns observed at the end of a 10 s simulation when the values for the coefficient of restitution used were 0.1 (corresponding to the last snapshot of Figure 3) and 1.0, respectively. It may be seen that particles form small clusters throughout the pipe but not a single large plug in the latter case. As such, the plug flow regime may not exist at high values of coefficient of restitution, and a low value such as that used throughout the present study is necessary to reproduce computationally both the dispersed and plug flow regimes observed in vertical pneumatic conveying.

Conclusions

The discrete element method utilizing a linear spring-dashpot-friction slider force-displacement model was coupled with computational fluid dynamics and used for the simulation of pneumatic conveying of granular material in both vertical and horizontal pipes in this study. The motions of solid particles and gas were obtained by time integration of Newton's second law of motion and the Navier-Stokes equations, respectively. Fluid drag forces were calculated using a fluid-particle drag force model and also represented as a source term in the gas momentum equation to ensure satisfaction of Newton's third law between the two phases. The effects of rolling friction and collision dynamics have also been considered in the computational model developed.

The simulation results obtained were in good agreement with previously reported experimental observations in terms of the types of flow patterns arising at different operating conditions used. In vertical pneumatic conveying, particles tend to be dispersed throughout the pipe at high gas velocities and low solid concentrations. On the other hand, particles tend to cluster together and move in the form of a dense plug when gas velocities are low or solid concentrations are high. These flow patterns have been referred to as the dispersed and plug flow regimes, respectively. The solid concentration profile for dispersed flow was observed to be symmetrical and with a minimum near the center of the pipe, while that for plug flow was almost flat. In horizontal pneumatic conveying, the simulations also show the presence of homogeneous or slug flow regimes, where particles are distributed along the length of the pipe or

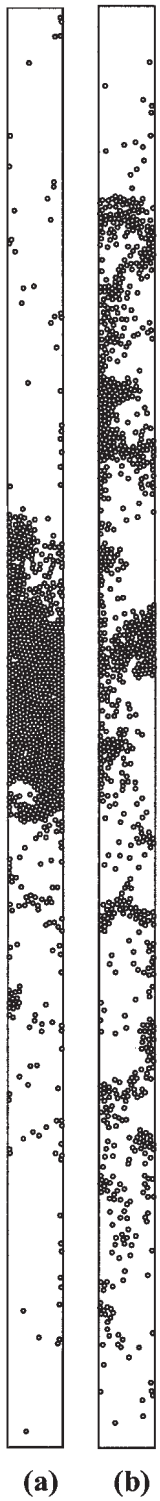

Figure 25. Comparisons of flow patterns obtained in vertical pneumatic conveying (gas velocity 14 m s^{-1}, $\alpha = 0.16$) for values of coefficient of restitution equal to (a) 0.1 and (b) 1.0.

Particles in the latter case do not show a tendency to cluster into a single large plug.

packed together as a large cluster, respectively. In addition, due to the effects of gravitational forces that cause particles to settle towards the bottom wall of the horizontal pipe, the stratified

and moving dunes flow regimes where particles are transported by traction along the pipe wall are observed at low gas velocities and solid concentrations. The solid concentration profile for stratified flow was unsymmetrical, with higher concentration near the lower wall of the pipe, while that for slug flow was similar to the flat profile seen for plug flow in vertical pneumatic conveying.

The various flow regimes and their corresponding operating conditions have been represented in the form of phase diagrams. In the range of gas velocity values where transition between two flow regimes might be taking place in a vertical pipe, hysteresis of the solid flow rates was observed to occur. The types of flow regimes obtained at the different operating conditions were observed to be insensitive to parameters used in the mathematical model within the range of values investigated in a sensitivity analysis of these parameters. However, the steady state solid flow rate showed a marginal decrease with increasing coefficient of friction. Solid particles with a low viscous contact damping coefficient or equivalently high coefficient of restitution have a low tendency to form large clusters, and the plug flow regime normally observed in vertical pneumatic conveying may not exist under such conditions. The mathematical model used in the present study may also be extended to include the effects of electrostatics or particle attrition to investigate the influences of such effects in pneumatic conveying systems in subsequent studies. In particular, it may be possible to simulate the few other types of flow regimes mentioned earlier that have been observed in physical experiments with the incorporation of such effects.

Acknowledgments

This study has been supported by the National University of Singapore under grant number R-279–000-095–112. EWCL and CHW acknowledge the use of supercomputing resources and an HPC Quest 2004 Silver Award jointly offered by IBM and the Institute of High Performance Computing, Singapore.

Literature Cited

1. Tashiro H, Peng X, Tomita Y. Numerical prediction of saltation velocity for gas-solid two-phase flow in a horizontal pipe. *Powder Technology*. 1997;91:141-146.
2. Huber N, Sommerfeld M. Modelling and numerical calculation of dilute-phase pneumatic conveying in pipe systems. *Powder Technology*. 1998;99:90-101.
3. Levy A. Two-fluid approach for plug flow simulations in horizontal pneumatic conveying. *Powder Technology*. 2000;112:263-272.
4. Cundall PA, Strack ODL. A discrete numerical model for granular assemblies. *Geotechnique*. 1979;29:47-65.
5. Tsuji Y, Tanaka T, Ishida T. Lagrangian numerical simulation of plug flow of cohesionless particles in a horizontal pipe. *Powder Technology*. 1992;71:239-250.
6. Tsuji Y, Kawaguchi T, Tanaka T. Discrete particle simulation of two-dimensional fluidized bed. *Powder Technology*. 1993;77:79-87.
7. Xu BH, Yu AB. Numerical simulation of the gas-solid flow in a fluidized bed by combining discrete particle method with computational fluid dynamics. *Chemical Engineering Science*. 1997;52:2785-2809.
8. Mikami T, Kamiya H, Horio M. Numerical simulation of cohesive powder behavior in a fluidized bed. *Chemical Engineering Science*. 1998;53:1927-1940.
9. Kaneko Y, Shiojima T, Horio M. DEM simulation of fluidized beds for gas-phase olefin polymerization. *Chemical Engineering Science*. 1999; 54:5809-5821.
10. Rhodes MJ, Wang XS, Nguyen M, Stewart P, Liffman K. Study of mixing in gas-fluidized beds using a DEM model. *Chemical Engineering Science*. 2001;56:2859-2866.
11. Li J, Mason DJ. A computational investigation of transient heat transfer in pneumatic transport of granular particles. *Powder Technology*. 2000;112:273-282.
12. Han T, Levy A, Kalman H. DEM simulation for attrition of salt during dilute-phase pneumatic conveying. *Powder Technology*. 2003;129:92-100.
13. Di Felice R. The voidage function for fluid-particle interaction systems. *International Journal of Multiphase Flow*. 1994;20:153-159.
14. Xu BH, Yu AB, Chew SJ, Zulli P. Numerical simulation of the gas-solid flow in a bed with lateral gas blasting. *Powder Technology*. 2000;109:13-26.
15. Zhou YC, Wright BD, Yang RY, Xu BH, Yu AB. Rolling friction in the dynamic simulation of sandpile formation. *Physica A*. 1999;269: 536-553.
16. Beer FP, Johnson ER. *Mechanics for Engineers—Statistics and Dynamics*. New York: McGraw-Hill, 1976.
17. Verlet L. Computer "experiments" on classical fluids. I. Thermodynamical properties of Lennard-Jones molecules. *Physical Review*. 1967;159:98-103.
18. Patankar SV. *Numerical Heat Transfer and Fluid Flow*. New York: Hemisphere, 1980.
19. Rao SM, Zhu K, Wang CH, Sundaresan S. Electrical capacitance tomography measurements on the pneumatic conveying of solids. *Industrial and Engineering Chemistry Research*. 2001;40:4216-4226.
20. Zhu K, Rao SM, Wang CH, Sundaresan S. Electrical capacitance tomography measurements on vertical and inclined pneumatic conveying of granular solids. *Chemical Engineering Science*. 2003;58:4225-4245.
21. Yao J, Zhang Y, Wang CH, Matsusaka S, Masuda H. Electrostatics of the granular flow in a pneumatic conveying system. *Industrial and Engineering Chemistry Research*. 2004;43:7181-7199.

Manuscript received Jan. 13, 2005, and revision received Jun 6, 2005.